ZnO NPs delay the recovery of psoriasis-like skin lesions through promoting inflammation and keratinocyte apoptosis via nuclear translocation of phosphorylated NF-κB p65 and cysteine deficiency

Xuan Lai
Southern Medical University Nanfang Hospital
Menglei Wang
Southern Medical University Nanfang Hospital
Yixia Zhu
Southern Medical University Nanfang Hospital
Xiaoli Feng
Southern Medical University Stomatological Hospital
Huimin Liang
Southern Medical University Nanfang Hospital
Li Nie
Southern Medical University Nanfang Hospital
Li Li
Southern Medical University Nanfang Hospital
Longquan Shao (shaolongquan@smu.edu.cn)
Southern Medical University Nanfang Hospital https://orcid.org/0000-0002-3770-0815

Research

Keywords: Zinc oxide nanoparticles, psoriasis-like skin, keratinocyte, inflammation, apoptosis, NF-κB p65, cysteine

Posted Date: April 17th, 2020

DOI: https://doi.org/10.21203/rs.3.rs-22538/v1

Abstract

Background

This study aimed to confirm the safety and risk of applying zinc oxide nanoparticles (ZnO NPs) to pathological skin, such as psoriasis-like skin. The majority of previous studies confirmed the safety of applying ZnO NPs to normal skin. However, we know very little about the risks of using sunscreen, cosmetics and topical drugs containing ZnO NPs for individuals with skin diseases. In addition, some studies claimed that ZnO NPs can penetrate normal or pathological skin, and ZnO NPs have frequently been reported to have proinflammatory and lethal effects in vitro. Therefore, it is necessary to evaluate the safety of applying ZnO NPs to pathological skin.

Results

ZnO NPs passed through gaps between keratinocytes and entered stratum basale of epidermis and dermis in imiquimod (IMQ)-induced psoriasis-like skin lesions. Application of a ZnO NP-containing suspension for 3 connective days delayed the healing of the epidermal barrier; increased the expression levels of inflammatory cytokines; promoted keratinocyte apoptosis and disturbed redox homeostasis. In vitro, ZnO NPs promoted TNF-α, IL-1β and IL-6 secretion and apoptosis of recombinant-human-TNF-α-stimulated HaCaT cells. NF-κB, ERK, p38 and JNK inhibitors blocked ZnO NP-induced inflammation. JSH-23, an inhibitor of the nuclear translocation of p-NF-κB p65, and NAC, an acetylated precursor of L-cysteine, not only inhibited the ZnO NP-induced inflammation but also inhibited apoptosis and cysteine deficiency. Neither erastin nor RSL3 induced p-NF-κB p65 nuclear translocation, but they did reduce cysteine biosynthesis. Additionally, ferropstatin-1, an inhibitor of lipid peroxidation, partially rescued ZnO NP-induced decreases in cell viability and cysteine content.

Conclusions

ZnO NPs delay the recovery of psoriasis-like skin lesions through promoting inflammation and keratinocyte apoptosis via the nuclear translocation of phosphorylated NF-κB p65 and cysteine deficiency. This work reminds the public that ZnO NPs are not safe for pathological skin, especially in inflammatory skin diseases such as psoriasis, and has revealed a partial mechanism by which ZnO NPs delay the recovery of pathological skin, promoting the appropriate use of ZnO NPs.

Background

For many years, zinc oxide (ZnO) has been widely used in food, pharmaceuticals, cosmetics and other chemicals used on a daily basis, and formulations of these products containing ZnO nanoparticles (ZnO NPs) are more popular than conventional formulations[1–4]. The content of ZnO NPs in certain topical drugs and cosmetics that frequently contact the skin is high. Previous studies claimed that ZnO NPs can

penetrate normal skin, but this finding was not confirmed by most other studies; additionally, pathological damage has not been found to result from topical ZnO NP application[5–7]. Therefore, it is generally believed that the topical application of ZnO NPs to normal human skin is safe. In fact, individuals with skin diseases, such as patients with psoriasis, atopic dermatitis (AD), acne and rosacea, use ZnO NP preparations at almost the same frequency as or at an even higher frequency than those with normal skin. These individuals often need to use medicinal or cosmetic ZnO NP preparations to treat diseases or cover unsightly skin. However, discussion on whether ZnO NPs are safe for pathological skin is limited, and the relevant guidelines do not provide definitive recommendations.

In skin diseases, the defects of skin barrier and the abnormal expression of barrier-related proteins in the epidermis are common[8, 9]. For example, both atopic dermatitis (AD) and psoriasis lead to the abnormal expression of filaggrin and loricrin, which are vital for the integrity of the physical barrier of the epidermis[10–12]. Theoretically, a defective barrier resulting from abnormal expression of barrier-related proteins is more permeable; moreover, in an AD mouse model, ZnO NPs have been reported to enter the dermis through the epidermis, inducing vigorous IgE production and suppressing inflammation[13]. This study indicated that ZnO NPs possess promising anti-inflammatory effects and can be used to treat inflammatory skin diseases. However, such results have been rarely observed in vitro. Most studies have reported that ZnO NPs have proinflammatory and lethal effects on keratinocytes and that oxidative stress is the main mechanism by which ZnO NPs injure cells[14–17]. These inconsistencies may be attributed to of the use of distinct ZnO NP dispersal systems or the features of different disease models.

In this study, psoriasis-like skin models were adopted to further elucidate the potential effects of ZnO NPs on pathological skin. Psoriasis is an inflammatory skin disease characterized by epidermal hyperplasia and excessive proliferation of keratinocytes[18]. The tumour necrosis factor-α (TNF-α)-nuclear factor-κB p65 (NF-κB p65) axis plays an important role in the inflammatory response and the excessive proliferation of keratinocytes in psoriasis[19]. The imiquimod (IMQ)-induced mouse model and TNF-α-stimulated HaCaT cell line are two classical models used to study psoriasis[20, 21]. Research on the IMQ-induced mouse model has demonstrated that ZnO NPs affect the progression or recovery of psoriasis-like skin lesions through their involvement in the inflammatory response, oxidative stress and apoptosis. In TNF-α-stimulated HaCaT cells, the effects of ZnO NPs on inflammatory keratinocytes have been evaluated by determining the levels of proteins and signalling molecules highly related to psoriasis and oxidative stress damage. The potential mechanism underlying the effects of ZnO NPs has also been discussed and mainly involves the nuclear translocation of phosphorylated NF-κB p65 (p-NF-κB p65) and cysteine deficiency. We believe that this work is enlightening, improves our understanding of the pathogenicity of ZnO NPs in abnormal skin and will be helpful for individuals with pathological skin conditions.

Results

Characterization of ZnO NPs

X-ray photoelectron spectroscopy (XPS) data were used to determine the composition of the ZnO NPs adopted in this study (Fig. 1A). Transmission electron microscopy (TEM) and scanning electron microscopy (SEM) images showed that the ZnO NPs were prism-shaped with a primary size of 41.34 ± 9.41 nm (Fig. 1B&C). The hydrodynamic sizes of the ZnO NPs in the suspension used for the animal experiments, complete medium and distilled water (DW) were 810.3 ± 116.5 nm, 189.0 ± 63.3 nm, and 266.7 ± 69.2 nm, respectively (Fig. 1D ~ F). The zeta potentials of the ZnO NPs in the suspension used for the animal experiments, complete medium and DW were 13.1 ± 0.5 mV, 11.9 ± 0.9 mV and 10.9 ± 0.2 mV, respectively (Table 3).

ZnO NPs delay the recovery of psoriasis-like skin lesions and penetrate the dermis

IMQ application for 6 consecutive days caused scales (Fig. 1G&H) and epidermal hyperplasia (Fig. 1I&J) on the dorsal skin. TEM images showed the intercellular gaps of approximately 2 μm between keratinocytes in IMQ-induced psoriasis-like skin lesions (Fig. 1K). These gaps disappeared after treatment with the suspension without ZnO NPs for 3 consecutive days (Fig. 1L) but remained when the suspension containing ZnO NPs was used. ZnO NPs entered epidermis through stratum corneum and were discovered in the nuclear of keratinocytes, stratum basale of epidermis and dermis (Fig. 1M ~ O). ICP-MS analysis confirmed that the elemental Zn content in the dermis of the ZnO NP-treated group was significantly higher than that in the negative control group (Fig. 1P).

ZnO NPs promote inflammation, apoptosis and oxidative stress in psoriasis-like skin lesions

The haemoxylin and eosin (H&E) staining results were similar for the negative control group and ZnO NP-treated group, but the ZnO NP-treated group exhibited a significantly greater number of inflammatory cells in the dermis than the negative control group (Fig. 2A&B). Immunohistochemical (IHC) analysis showed that ZnO NPs significantly increased the expression of TNF-α, interleukin (IL)-1β, IL-6 and cyclooxygenase 2 (COX2) in the epidermis and apparently increased the expression of IL-1β, IL-6 and COX2 in the dermis (Fig. 2C ~ J). Consistently, the mRNA levels of inflammatory cytokines were elevated in the full-thickness skin of the ZnO NP-treated group (Fig. 2K). Additionally, ZnO NPs significantly enhanced the level of TdT-mediated dUTP nick-end labelling (TUNEL; a biomarker of apoptosis) and 8-OHdG (a biomarker of DNA damage related to oxidative stress) staining in psoriasis-like skin lesions, especially in the epidermis (Fig. 2L ~ O), and disturbed redox homeostasis, as revealed by decreases in the total glutathione (T-GSH) content, reduced glutathione (GSH) content, GSH/oxidized glutathione (GSSH) ratio and glutathione peroxidase (GPx) content as well as an increase in the malondialdehyde (MDA) content (Fig. 2P ~ T).

ZnO NPs affect recombinant human TNF-α (rh-TNF-α)-stimulated HaCaT cells in a predominantly dose-dependent manner

The Cell Counting Kit-8 (CCK-8) assay showed that rh-TNF-α stimulation increased HaCaT cell proliferation and that cell viability began to decrease following treatment with 30 or 40 μg/mL ZnO NPs for 6 h (Fig. 3A). ZnO NPs also increased the levels of reactive oxygen species (ROS) and MDA (Fig. 3B&C) and decreased the T-GSH content, GSH content and cysteine level (Fig. 3D&E) in a similar dose-dependent manner. TEM images showed that rh-TNF-α stimulation led to no obvious changes in the ultrastructure of HaCaT cells (Fig. 3F&G) and that ZnO NPs were engulfed by rh-TNF-α-stimulated HaCaT cells and caused mitochondrial swelling and mitochondrial cristae destruction (Fig. 3H ~ I).

ZnO NPs promote inflammation and apoptosis and activate related pathways in rh-TNF-α-stimulated HaCaT cells

The mRNA levels of inflammatory cytokines were evaluated by quantitative real-time PCR (q-RT-PCR) analysis. ZnO NPs (30 or 40 μg/mL for 3 or 6 h) increased the mRNA levels of TNF-α, IL-1β and IL-6 (Fig. 3J&K). Inflammatory cytokines in the medium supernatant were quantified by enzyme-linked immunosorbent assay (ELISA). ZnO NPs (20 ~ 40 μg/mL for 6 h) promoted the secretion of TNF-α, IL-1β and IL-6 (Fig. 3L ~ N). At a ZnO NP concentration of 40 μg/mL, the secretion of IL-1β no longer continued to rise and plateaued at the level observed after treatment with 30 μg/mL ZnO NPs. In Annexin-V/propidium iodide (PI) analysis, points in the right lower quadrant (Q4) represent early apoptotic cells, and points in the right upper quadrant (Q2) represent late apoptotic cells and necrotic cells. The proportion of early apoptotic cells (Q4) increased from 0.8% in cells incubated with 30 μg/mL ZnO NPs for 6 h to 7.9% in those incubated with 40 μg/mL ZnO NPs for 6 h, and the proportion of late apoptotic cells and necrotic cells (Q2) increased from 7.1–24.1% under these conditions (Fig. 3O). Western blotting of total protein showed that ZnO NPs (30 or 40 μg/mL for 3 ~ 12 h) increased the phosphorylation of NF-κB, extracellular-regulated protein kinase (ERK), p38 and c-Jun N-terminal kinase (JNK) (Fig. 4A ~ E), the ratio of BAX/Bcl-2, and cleaved-caspase 3 level (Fig. 4H ~ J). Fluorescence images showed that ZnO NPs (40 μg/mL for 6 h) strongly induced nuclear translocation of p-NF-κB p65 (Fig. 4F). Western blotting of the nuclear protein showed that ZnO NPs (30 or 40 μg/mL for 3 or 6 h) increased the level of nuclear p-NF-κB p65 (Fig. 4G).

Strong nuclear translocation of p-NF-κB p65 is involved in ZnO NP-induced inflammation, apoptosis and cysteine deficiency.

Quinazoline (QNZ) and JSH-23 inhibited p-NF-κB p65 nuclear translocation and ERK phosphorylation induced by ZnO NPs (40 μg/mL for 6 h). JSH-23 also apparently inhibited JNK phosphorylation (Fig. 5A&B). SCH772984, SB203580 and JNK-IN-8 inhibited ZnO NP-induced phosphorylation of ERK, p38 and JNK, respectively (Fig. 5B). NF-κB and mitogen-activated protein kinase (MAPK) inhibitors blocked ZnO NP-induced TNF-α, IL-1β and IL-6 secretion, but JNK-IN-8 did not inhibit ZnO NP-induced IL-1β secretion (Fig. 5C ~ E). NAC, an N-acetyl derivative of cysteine, almost entirely inhibited the changes induced by ZnO NPs (40 μg/mL for 6 h), including the decreased in cell viability (Fig. 5F) and the increase in TNF-α, IL-1β and IL-6 secretion (Fig. 5C ~ E); MAPK phosphorylation (Fig. 5B); p-NF-κB p65 nuclear translocation; caspase 3 activation and the BAX/Bcl-2 ratio (Fig. 5G). ZnO NP-induced decreases in cell viability (Fig. 9F) and cellular cysteine content (Fig. 5H) were also reversed by JSH-23.

Cysteine deficiency is involved in ZnO NP-induced apoptosis and is mediated by ROS and lipid peroxidation.

The CCK-8 assay revealed that cell viability was decreased by RSL3 but not by erastin (Fig. 5I). Both erastin and RSL3 decreased the cysteine content, but cysteine levels were lower in the RSL3-treated group than in the erastin-treated group (Fig. 5J). Erastin and RSL3 did not increase the nuclear p-NF-κB p65 level, but RSL3 increased the ratio of BAX/Bcl-2. Erastin, RSL3 and ZnO NPs did not affect xCT expression and decreased CD98 expression. The decrease in CD98 expression induced by erastin was less pronounced than that induced by RSL3 or ZnO NPs. The expression of CBS was significantly increased by erastin and was only slightly increased by RSL3 and ZnO NPs. The expression of CTH was significantly increased by erastin and ZnO NPs and was strongly increased by RSL3 (Fig. 5K).

Ferrostatin-1 (Fer-1) and NAC inhibited the ZnO NP-induced decline in cell viability and cysteine content, but Fer-1 was less effective than NAC (Fig. 5I&J). Fer-1 and NAC also inhibited ZnO NP-induced alterations, including the increases in the nuclear p-NF-κB p65 level; caspase 3 activation; the BAX/Bcl-2 ratio; and TNF-α, IL-1β and IL-6 secretion and the decrease in the CD98 level (Fig. 5K ~ N). Deferiprone (DEP) did not rescue the ZnO NP-induced decline in cell viability or cysteine content (Fig. 5I&J) but inhibited the increase in the BAX/Bcl-2 ratio and the decrease in the CD98 level (Fig. 5K). Z-VAD-FMK (ZVF) did not rescue the ZnO NP-induced decline in cysteine content (Fig. 5J) but inhibited these ZnO NP-induced changes, including the decrease in cell viability (Fig. 5I), caspase 3 activation, and the increases in the BAX/Bcl-2 ratio (Fig. 5K) and IL-1β and IL-6 secretion (Fig. 5L ~ N).

Discussion

To confirm the effects of ZnO NPs on pathological skin, an IMQ-induced psoriasis-like skin model was adopted in this study. After IMQ was topically applied for connective 6 days, the skin was covered with scales, and H&E staining showed epidermal hyperplasia; these findings demonstrated that a psoriasis-like skin model had been established. TEM images revealed abundant gaps of approximately 2 μm between keratinocytes that allowed nanomaterials to pass and enter the deep layers of the epidermis and dermis

in this IMQ-induced psoriasis-like skin model. Similarly, a previous study reported that ZnO NPs enter the dermis through the epidermis in an AD model[13]. Although characterization of the ZnO NPs indicated that they tended to agglomerate and that ZnO NP suspensions should be ultrasonically dispersed before use, the agglomerated ZnO NPs were still able to penetrate through these gaps in the epidermis and reached to stratum basale of epidermis and dermis. Additionally, TEM images of cells displayed the ability of keratinocytes to phagocytose ZnO NPs. All of the above results indicate the risks of applying topical drugs and cosmetics containing ZnO NPs to pathological skin.

In a further experiment, we applied a ZnO NP suspension to the IMQ-induced psoriasis-like skin model at a single exposure dose of 1.67 mg/cm^2 for 3 consecutive days. This dose is lower than the effective concentration of ZnO NPs in sunscreen (2 mg/cm^2)[22]. The IMQ-induced psoriasis-like skin model is reversible[23, 24]. This means that the defective epidermal barrier can spontaneously recover. We found that application of ZnO NPs delayed the recovery of psoriasis-like skin lesions and induced inflammation, apoptosis and oxidative stress in the epidermis and dermis. In the negative control group, the gaps between keratinocytes disappeared after 3 days of treatment, whereas these gaps remained in the ZnO NP-treated group. In psoriasis, IL-1 is likely to initiate the inflammatory response and cause dysfunction of keratinocytes; furthermore, TNF-α, IL-1 and IL-6 derived from dysregulated keratinocytes amplify the inflammatory response through promoting the differentiation of myeloid dendritic cells[19, 25, 26]. IL-17A and IL-22 released by activated lymphocytes mediate chronic inflammation in psoriasis[21, 27–29]. In psoriasis, high expression of COX2 is associated with a persistent inflammatory response[19, 30]. The enhancement of TNF-α, IL-1β, IL-6 and COX2 expression levels and the increase in the transcription of inflammatory cytokines, including TNF-α, IL-1β, IL-6, IL-17A and IL-22, in the ZnO NP-treated group indicated that ZnO NPs may hinder the anti-inflammatory effect of drugs used to treat these diseases.

More importantly, the higher level of TUNEL staining in the ZnO NP-treated group implied that keratinocyte apoptosis was increased and that the histological foundation for epidermal renewal capacity was impaired. Oxidative stress is generally thought to play a pivotal role in the mechanism by which nanomaterials damage cells[31]. The higher level of 8-OHdG staining in the ZnO NP-treated group revealed that ZnO NPs promoted DNA damage related to oxidative stress in pathological keratinocytes. GSH prevents proteins from being damaged by ROS by oxidizing their own thiol groups[32]. The MDA level indicates the extent of lipid peroxidation[31]. The disturbance of GSH antioxidant system and the increased MDA level in the ZnO NP-treated group revealed the potential mechanism by which ZnO NPs promote inflammation and keratinocyte apoptosis in pathological skin.

Keratinocytes are essential for the integrity of the epidermal barrier, which plays an important role in maintaining skin health. It is necessary to elucidate how ZnO NPs affect keratinocytes in pathological skin. An rh-TNF-α stimulated (10 ng/mL for 48 h) HaCaT cell model, the most common in vitro model of psoriasis, was adopted for further experiments. As expected, rh-TNF-α stimulation increased cell viability and the secretion of inflammatory cytokines, and subsequent treatment with ZnO NPs damaged the rh-TNF-α-stimulated HaCaT cells in a predominantly dose-dependent manner. When the concentration of ZnO NPs was below 10 μg/mL, the secretion of inflammatory cytokines and cell viability were not

affected in the short term. When the concentration of ZnO NPs reached 20 μg/mL, IL-1β and IL-6 secretion began to be increased, and cell viability was significantly increased after 48 h, but not after 24 h, of treatment. If this increase in cell viability is due to ZnO NP-induced inflammation, a middle dose of ZnO NPs may aggravate epidermal hyperplasia in psoriasis. TNF-α and IL-1β secretion and ROS levels peaked after treatment with 30 μg/mL ZnO NPs. At a ZnO NP concentration of 40 μg/mL, IL-6 secretion continued to increase, cell viability and the cysteine level dramatically decreased, and the proportion of apoptotic cells revealed by Annexin V/PI analysis was significantly increased. These findings show that 30 ~ 40 μg/mL is the initial dose at which ZnO NPs can simultaneously promote inflammation and apoptosis. This result is consistent with the phenomena observed in vivo; thus, this dose was adopted for the subsequent experiments.

TNF-α inhibition or antagonism is an important therapeutic strategy for the treatment of psoriasis and the production and secretion of TNF-α is associated with NF-κB and MAPK pathways[33, 34]. The TNF-α-NF-κB axis is involved in the epidermal hyperplasia and inflammatory response in psoriasis[35, 36]. MAPK not only participates in the inflammatory response in psoriasis but also plays a part in the nanomaterial-induced stress response[31]. Treatment with 40 μg/mL ZnO NPs for 6 h induced strong nuclear translocation of p-NF-κB p65 and MAPK activation; enhanced phosphorylation of ERK, p38 and JNK was observed and was accompanied by enhancement of the inflammatory response. These results suggest that ZnO NPs aggravate psoriasis by promoting the inflammatory response via NF-κB and MAPK activation. Indeed, our results indicated that inhibitors of NF-κB and MAPK block the proinflammatory effect of ZnO NPs on rh-TNF-α-stimulated HaCaT cells.

The inflammatory response is responsible for keratinocyte proliferation and epidermal hyperplasia in psoriasis. The roles of NF-κB in promoting inflammation and inhibiting apoptosis have been acknowledged, and inhibitors of NF-κB are frequently used to protect against the inflammatory response and excessive proliferation[19, 36]. However, we unexpectedly found that two inhibitors of NF-κB, QNZ and JSH-23, had opposing effects on the ZnO NP-induced decline in cell viability. Generally, NF-κB activation begins with IκBα degradation, which is followed by a regulated series of steps in a cascade in the cytoplasm and the nuclear translocation and binding of NF-κB to DNA. According to the literature, QNZ is a potent inhibitor of NF-κB and inhibits the production of TNF-α[37]. In contrast, JSH-23 inhibits the nuclear translocation of NF-κB p65 without affecting IκBα degradation[38]. In this study, QNZ had a more thorough inhibitory effect on the NF-κB activation and p-NF-κB p65 nuclear translocation than JSH-23. As a result, the decline in cell viability and apoptosis mediated by the mitochondrial pathway (increased BAX/Bcl-2 ratio) and the caspase family (increased cleaved-caspase 3 level) were rescued by JSH-23 but not QNZ. This suggests that the strong nuclear translocation of p-NF-κB p65 is involved in ZnO NP-induced apoptosis and that excessive inhibition of the NF-κB pathway is not conducive to preventing the pro-apoptotic effect of ZnO NPs on keratinocytes. Moreover, NF-κB inhibitors are commonly used for the treatment of inflammatory skin diseases. Thus, the addition of ZnO NPs to sunscreens or medicines may affect the efficacy of these drugs.

It has been acknowledged that nanomaterials tend to mediate oxidative stress, and this effect may explain the potential risk of nanomaterials or be used to promote their application in some fields[39–42]. NAC is a general inhibitor of ROS. More precisely, NAC is an acetylated precursor of cysteine, which is deacetylated in cells and become cysteine[43–45]. In this study, NAC efficiently inhibited ZnO NP-induced inflammation, apoptosis and activation of related pathways, including the increase in the level of nuclear p-NF-κB p65. In addition, we found that ZnO NP-induced cysteine deficiency was partially reversed by JSH-23, an inhibitor NF-κB p65 nuclear translocation. Therefore, it can be inferred that ZnO NP-induced cysteine deficiency is related to the nuclear translocation of p-NF-κB p65. However, erastin and RSL3 did not induce the nuclear translocation of p-NF-κB p65 in rh-TNF-α-stimulated HaCaT cells though they inhibited cysteine biosynthesis. This suggests that cysteine deficiency is involved in ZnO NP-induced apoptosis and is mediated by the strong nuclear translocation of p-NF-κB p65 induced by ZnO NPs. Additionally, erastin and RSL3 did not promote inflammatory cytokine secretion.

Cysteine is an essential donor of sulfhydryl in the biosynthesis of GSH and plays a decisive role in cell survival[32]. ZnO NP-induced cysteine deficiency means the imbalance of antioxidant system. The cysteine/glutamate amino acid transporter system x_c^-, which consists of CD98 and xCT, is the main system by which cysteine is synthesized[46]. Certain types of cells can biosynthesize cysteine through the transsulfuration pathway, of which CBS and CTH are the rate-limiting enzymes of the first and last steps, respectively[47–49]. In this study, erastin, RSL3 and ZnO NPs decreased CD98 expression. However, erastin significantly increased CBS and CTH levels and did not cause cell death though reducing cysteine content. RSL3 and ZnO NPs increased the level of CTH and caused apoptosis and a relatively severe cysteine deficiency. These results suggest that when system x_c^- is impaired, keratinocytes can utilize the transsulfuration pathway to generate cysteine; however, cysteine deficiency and related cell death cannot be prevented by promoting only the last step of the transsulfuration pathway. Besides, previous studies claimed that cysteine is an endogenous metal ion chelator[50, 51]. Therefore, NAC not only maintains the antioxidant system by providing sufficient sulfhydryl, but also can chelate ZnO NPs or Zn^{2+} to alleviate ZnO NP-induced cell damage. In addition, Fer-1, an inhibitor of lipid peroxidation, is effective for preventing ZnO NP-induced cell damage. All of the above results imply that oxidative stress and lipid peroxidation are involved in ZnO NP-induced damage to keratinocytes and that an available antioxidant system is essential for the survival and health of keratinocytes exposed to ZnO NPs.

Conclusions

In summary, this work demonstrated that ZnO NPs can delay the recovery of psoriasis-like skin lesions through promoting the inflammatory response and keratinocyte apoptosis and that ZnO NPs can lead to further inflammation and TNF-α-stimulated keratinocyte apoptosis via strong nuclear translocation of p-NF-κB p65 and cysteine deficiency. Although we have considered whether ZnO NPs can be used to suppress epidermal hyperplasia, we ultimately believe that ZnO NPs are not desirable because they are likely to prevent the proliferation of normal keratinocytes and epidermal barrier regeneration. Based on the above, it can be concluded that ZnO NPs are not safe for pathological skin. Moreover, the evidence

provided here is enlightening and improves our understanding of the pathogenicity of ZnO NPs in abnormal skin.

Methods

Preparation and characterization of ZnO NP suspensions

The composition, shape and primary size of ZnO NPs (50 nm; CAS number:1314-13-2, SigmaAldrich, USA) were determined by XPS (D8 advanced, Bruker, Germany), SEM (Sigma 500, Zeiss, Germany) and TEM (Tecnai G2 F20, FEI, USA), respectively. The hydrodynamic size and zeta potentials of the ZnO NPs were determined with a Malvern Zetasizer (Nano-ZS, Malvern, UK).

To prepare a suspension for the animal experiments, ZnO NPs were dispersed in normal saline (NS) containing 1% hydroxy propyl methyl cellulose (HPMC) at a concentration of 20 mg/mL. HPMC was used as a suspension agent to ensure that the nanoparticles were uniformly dispersed and to increase operability. The suspension was ultrasonically dispersed in an ice bath for 30 min before each use.

To prepare a stock solution for the cell experiments, ZnO NPs were dispersed in phosphate-buffered saline (PBS) at a concentration of 2 mg/mL and autoclaved. The working solution was the stock solution diluted 4 times with basic medium and was ultrasonically dispersed in an ice bath for 15 min before each use.

Animals and treatments

6-week-old female C57BL/6 mice were purchased from the Animal Center of Southern Medical University (Guangdong, China). The mice were housed in a room free of specific pathogens (23 ± 1 °C room temperature, 60 ± 10% relative humidity) and underwent an adaptation period for one week before treatment.

A 6-cm^2 area of the dorsal skin was shaved, and 62.5 mg of IMQ (Med-Shine, China) was topically applied daily from the 1st day to the 6th day to establish a psoriasis model. After model establishment as histologically confirmed, the mice were randomly distributed into 2 groups of 8 mice per group. From the 7th to the 9th day, 500 μL of NS (containing 1% HPMC) or a ZnO NP suspension (consisting of NS, 1% HPMC and ZnO NPs) was topically applied twice daily to the negative control group and the ZnO NP-treated group, and the mice were sacrificed on the 10th day.

TEM observation of the epidermis

Skin tissues (1×2 mm^2) in area were cut from the central area of the freshly excised dorsal skin using a sharp surgical blade, immersed in 2.5% glutaraldehyde overnight at 4 °C, processed and embedded in

resin. The micromorphology of the tissues was observed using TEM (H-7500, Hitachi, Japan).

Inductively coupled plasma mass spectra (ICP-MS) analysis of the dermis

The dorsal skin was cleaned with NS at room temperature, excised and placed in 0.2% dispase II protease (Sigma-Aldrich, USA) overnight at 4 °C. The epidermis was removed, and the dermis was gently rinsed in precooled NS 3 times and dried with clean filter paper. 2 g of each dermis sample was digested with nitric acid and hydrogen peroxide through microwave heating at 160 °C. Then, the samples were heated at 120 °C overnight to fully evaporate the nitric acid. The final solutions were diluted to 2 mL with 1% nitric acid and 0.1% Triton-100 and analysed by ICP-MS (7700s, Agilent, USA).

Histopathological examination

Freshly excised dorsal skin pieces were immersed in 4% paraformaldehyde for 24 h and embedded in paraffin wax after dehydration using graded ethanol and xylene solutions. The tissues were sliced at a thickness of 4 μm. H&E staining was performed for histological morphological analysis. IHC was used to detect the number of TUNEL (Servicebio, China)-labelled cells and the levels of 8-OHdG (JaICA, Japan), TNF-α (Abcam, USA), IL-1β (Abcam, USA), IL-6 (Abcam, USA) and COX2 (Bimake, USA). Images were captured using a microscope (BX63, Olympus, Tokyo, Japan). Cell counts and grey value analysis were performed using ImageJ software.

qRTPCR analysis of the inflammatory response in vivo

Skin tissues that had been frozen in liquid nitrogen and stored at -80 °C were homogenized in liquid nitrogen and extracted with TRIzol reagent (Gibco, USA) according to the manufacturer's instructions. The concentration and purity of the total RNA were determined by measuring the absorbance at 260 and 280 nm using a spectrophotometer (Molecular Devices, USA). Complementary DNA (cDNA) was reverse transcribed from mRNA samples using a PrimeScript™ RT Reagent Kit (TaKaRa, Japan). qRTPCR was performed with a LightCycler 480 Sequence Detector System (Roche, Switzerland) using a commercial kit (SYBR Premix Ex Taq II, TaKaRa, Japan). The mouse primer sequences used for qRT-PCR are shown in Table 1.

Measurements of oxidative stress biomarkers

Skin tissues that had been frozen in liquid nitrogen and stored at -80 °C were homogenized in precooled NS using a tissue homogenizer. The homogenates (1:10 w/v) were centrifuged at 3000 rpm for 10 min at 4 °C to obtain supernatants. The protein concentrations of the supernatants were determined with a BSA

kit (Thermo Fisher, USA). T-GSH, GSH, and GSSH levels, GPx levels, and MDA levels were quantified with a GSH and GSSH assay kit (Beyotime, China), a GSH peroxidase assay kit (Beyotime, China) and an MDA assay kit (Nanjing Jiancheng Bioengineering Institute, China), respectively, according to the manufacturer's instructions.

Cell culture and treatments

Normal human immortalized keratinocytes (HaCaT cells) were obtained from Otwo Biotech, Inc. (Shenzhen, China). Cell line authentication by short tandem repeat (STR) profiling indicated that this cell line matched the HaCaT cell line (code: 711) collected by Deutsche Sammlung von Mikroorganismen und Zellkulturen (DSMZ). The cells were cultured in Dulbecco's modified Eagle medium (4.5 g of L-glucose/L) containing 10% foetal bovine serum at 37 °C in a 5% CO_2 humidified incubator. The culture medium was replaced every other day, and the cells were passaged when they reached approximately 90% confluence.

HaCaT cells were stimulated with rh-TNF-α (10 ng/mL for 48 h; R&D, USA) to establish an in vitro model of psoriasis. The medium supernatant was collected after rh-TNF-α stimulation and used to dilute the sonicated ZnO NP working solution. rh-TNF-α-stimulated HaCaT cells continued to be cultured in diluted ZnO NP working solution containing 10, 20, 30 or 40 μg/mL ZnO NPs for 1, 3, 6, 12 or 24 h.

Inhibitor application

Cells were pretreated with inhibitors of the NF-κB and MAPK pathways and oxidative stress for 3 h before ZnO NP treatment for 6 h to determine the mechanism by which ZnO NPs promote inflammation and cell death. QNZ (0.1 μM; TargetMol, USA) is an inhibitor of NF-κB activation and TNF-α production. JSH-23 (10 μM; TargetMol, USA) suppresses the nuclear translocation and transcriptional activity of NF-κB. SCH772984 (10 μM; TargetMol, USA), SB203580 (2 μM; TargetMol, USA) and JNK-IN-8 (1 μM; TargetMol, USA) inhibit the phosphorylation of ERK, p38 and JNK, respectively. N-acetylcysteine (NAC, 1 mM; TargetMol, USA), the N-acetyl derivative of cysteine, inhibits ROS.

To understand the role of cysteine and oxidative stress in the mechanism by which ZnO NPs induce apoptosis, inhibitors of cysteine synthesis and antioxidants were applied. Erastin (200 μM; TargetMol, USA) inhibits the cysteine/glutamate amino acid transporter system x_c^-, which is the main pathway of cysteine biosynthesis. RSL3 (10 μM; TargetMol, USA) inhibits cysteine synthesis and is a covalent inhibitor of glutathione peroxidase 4. Cells not treated with ZnO NPs were treated with erastin and RSL3 for 6 h. Fer-1 (20 μM; TargetMol, USA) blocks lipid peroxidation. DEP (40 μM; MCE, USA) depletes iron and prevents iron-dependent lipid peroxidation. ZVF (30 μM; Selleck, USA) is an irreversible pan-caspase inhibitor. NAC (1 mM) was also used to inhibit ROS. Cells treated with ZnO NPs were treated with Fer-1, DEP, ZVF and NAC for 6 h.

Cell survival assay

The cells were seeded in 96-well plates at a density of 2000 cells per well and allowed to attach overnight. Then, the cells were treated with rh-TNF-α and ZnO NPs. Cell viability was determined using a CCK-8 assay kit (Dojindo Molecular Technologies, Japan), and the absorbance was measured at a wavelength of 450 nm using a microplate reader.

TEM observation of cells

rh-TNF-α and ZnO NP (40 μg/mL for 6 h)-treated cells were washed with 37 °C PBS and fixed with 2.5% glutaraldehyde. The fixed cells were collected using a cell scraper and centrifuged at 1000 g for 5 min at 4 °C. The samples were then embedded, and ultrathin slices were prepared. Intracellular structural changes were observed using a Hitachi H-7500 TEM instrument (Hitachi, Japan).

Cellular ROS assay

Cellular ROS production was determined by using 2',7'-dichlorofluorescin diacetate (DCFH-DA) probes (Beyotime, China). The treated cells were washed, collected with EDTA-free trypsin and incubated with the probes (10 μM) for 30 min at 37 °C, washed twice with PBS and resuspended in 500 μL of PBS. The fluorescence intensity of the cells was analysed using a flow cytometer (FACSAria III, BD, USA) at excitation/emission wavelengths of 485/535 for DCFH-DA.

Measurements of cellular GSH and cysteine levels

Cells were lysed and collected. T-GSH and GSH levels and cysteine levels were quantified with a GSH and GSSH assay kit (Beyotime, China) and a cysteine assay kit (Solarbio, China), respectively, according to the manufacturer s' instructions.

ELISA and q-RT-PCR analysis of the inflammatory response in vitro

The medium supernatant was collected and centrifuged at 5000 rpm for 10 min at 4 °C. The levels of TNF-α, IL-1 and IL-6 in the medium supernatant were quantified using ELISA kits (BioLegend, USA) according to the manufacturer's instructions. The cells were lysed with TRIzol reagent (Gibco, USA) according to the manufacturer's instructions. mRNA extraction, cDNA synthesis and qRT-PCR were carried out as described for the animal experiments. The human primer sequences used for qRT-PCR are shown in Table 2.

Annexin V/PI analysis

Cells were washed, digested with EDTA-free trypsin and stained with FITC-conjugated Annexin V and PI (Beyotime, China) according to the manufacturer's instructions. The final cell suspensions in PBS were analysed using flow cytometry (FACSAria III, BD, USA).

Immunofluorescence examination

The cells were seeded on slides, treated with rh-TNF-α and ZnO NPs, fixed with 4% paraformaldehyde overnight and permeabilized with 0.5% Triton X-100 for 30 min. After being blocked with 5% FBS for 1 h, the cells were incubated with an anti-p-NF-κB p65 antibody (CST, USA) at 4 °C overnight and incubated with a FITC-conjugated secondary antibody (Proteintech, China) at room temperature for 1 h. Fluorescence images were captured using a fluorescence microscope (BX63, Olympus, Tokyo, Japan).

Western blot analysis

Cells were collected and lysed using reagent from a nuclear protein and cytoplasmic protein extraction kit (Beyotime, China) containing 1 mM protease and phosphatase inhibitor (Beyotime, China). The cell lysates were heated in SDS-PAGE sample buffer (Genstar, China) at 99 °C for 5 min. The proteins were separated by SDS-PAGE and transferred to polyvinylidene difluoride membranes (Merck Millipore, Germany) that were then blocked with 5% skim milk for 1 h. The membranes were incubated overnight at 4 °C with primary antibodies, including anti-NF-κB p65, phospho-NF-κB p65, phospho-44/42 MAPK, phospho-p38, phospho-JNK, Bcl-2, cleaved-caspase 3 (CST, USA), ERK, p38, JNK, BAX, CD98, CBS, CTH, TBP, GAPDH (Proteintech, China), and xCT (Bimake, USA) antibodies. The membranes were then washed with TBST and incubated at room temperature with horseradish peroxidase (HRP)-conjugated secondary antibodies (CST, USA) for 1 h. Proteins were detected using an ECL kit (WBLKS0500, Merck Millipore, USA) and an automatic chemiluminescence image analysis system (Tanon, China). Quantitative analysis was performed using ImageJ software.

Statistical analysis

All the data are presented as the mean ± standard deviation (SD) and were analysed with SPSS 22.0 software. Comparisons among each group were assessed using one-way ANOVA when the variance in the data was homogenous or using a non-parametric test when the variance in the data was not homogenous. Differences for which $P < 0.05$ were considered to be statistically significant.

Abbreviations

ZnO NPs: zinc oxide nanoparticles; IMQ: imiquimod; AD: atopic dermatitis; NS: normal saline; HPMC: hydroxy propyl methyl cellulose; PBS: phosphate-buffered saline; SEM: scanning electron microscopy; TEM: transmission electron microscopy; XPS: X-ray photoelectron spectra; DLS: dynamic light scattering; DW: distilled water; ICP-MS: inductively coupled plasma mass spectra; H&E: hemoxylin and eosin; IHC: immunohistochemistry; q-RT-PCR: quantitative real-time polymerase chain reaction; ELISA: enzyme-linked immuno-absorbent assay; TNF-α: tumour necrosis factor-α; IL-1β: interleukin-1β; IL-6: interleukin-6; COX2: cyclooxygenase 2; TUNEL: TdT-mediated dUTP nick-end labelling; 8-OHdG: 8-hydroxy-2-deoxyguanosine; T-GSH: total-glutathione; GSH: reduced glutathione; GSSH: oxidized glutathione; GPx: glutathione peroxidase; MDA: malonaldehyde; ROS: reactive oxygen species; NF-κB：nuclear factor-κB; MAPK: mitogen-activated protein kinase; CBS: cystathionine β-synthase; CTH: γ-cystathionase; NAC: N-acetylcysteine; Fer-1: ferrostatin-1; DEP: deferiprone; ZVF: Z-VAD-FMK; HRP: horseradish peroxidase

Declarations

Ethics approval and consent to participate

All animal experiments were performed in compliance with the regulations and guidelines of the National Ethics Committee on Animal Welfare of China. This experiment was approved by the Nanfang Hospital Animal Ethics Committee with the approval number NFYY-2017-47.

Consent for publication

Not applicable.

Availability of data and materials

The datasets generated and analysed during the current study are available from the corresponding author on reasonable request. Online supporting information are available.

Competing interests

The authors declare that they have no competing interests.

Funding

This work was supported by the National Natural Science Foundation of China (51672122, 81870786), the Natural Science Foundation of Guangdong Province (2018A030313773) and the President Foundation of Nanfang Hospital, Southern Medical University (2016B007, 2018Z017, 2019C011).

Authors' contributions

All authors contributed to this study. XL, XF, LL and SL contributed to the idea and design of this article. XL, MW and HL performed the animal experiments. XL, YZ and LN performed the cell experiments. XL

and XF discussed the findings. XL wrote the draft manuscript. LL and LS revised the manuscript. All authors read and approved the final manuscript.

Acknowledgements

Not applicable.

References

1. Schneider SL, Lim HW. A review of inorganic UV filters zinc oxide and titanium dioxide. Photodermatol Photoimmunol Photomed. 2019;35 6:442–6.
2. Osmond MJ, McCall MJ. Zinc oxide nanoparticles in modern sunscreens: an analysis of potential exposure and hazard. Nanotoxicology. 2010;4 1:15–41.
3. Mohandas A, Kumar PTS, Raja B, Lakshmanan VK, Jayakumar R. Exploration of alginate hydrogel/nano zinc oxide composite bandages for infected wounds. Int J Nanomedicine. 2015;10(Suppl 1):53–66.
4. Aditya A, Chattopadhyay S, Jha D, Gautam HK, Maiti S, Ganguli M. Zinc oxide nanoparticles dispersed in ionic liquids show high antimicrobial efficacy to skin-specific bacteria. ACS Appl Mater Interfaces. 2018;10 18:15401–11.
5. Osmond-McLeod MJ, Oytam Y, Kirby JK, Gomez-Fernandez L, Baxter B, McCall MJ. Dermal absorption and short-term biological impact in hairless mice from sunscreens containing zinc oxide nano- or larger particles. Nanotoxicology. 2013;8(Suppl 1):72–84.
6. Gulson B, McCall M, Korsch M, Gomez L, Casey P, Oytam Y, Taylor A, McCulloch M, Trotter J, Kinsley L, Greenoak G. Small amounts of zinc from zinc oxide particles in sunscreens applied outdoors are absorbed through human skin. Toxicol Sci. 2010;118 1:140–9.
7. Labouta HI, Schneider M. Interaction of inorganic nanoparticles with the skin barrier: current status and critical review. Nanomedicine. 2013;9 1:39–54.
8. Medgyesi B, Dajnoki Z, Beke G, Gaspar K, Szabo IL, Janka EA, Poliska S, Hendrik Z, Mehes G, Torocsik D, Biro T, Kapitany A, Szegedi A. Rosacea is characterized by a profoundly diminished skin barrier. J Invest Dermatol. 2020.
9. Milner JD. Primary atopic disorders. Annu Rev Immunol. 2020.
10. Thyssen JP, Jakasa I, Riethmüller C, Schön MP, Braun A, Haftek M, Fallon PG, Wróblewski J, Jakubowski H, Eckhart L, Declercq W, Koppes S, Engebretsen KA, Bonefeld C, Irvine AD, Keita-Alassane S, Simon M, Kawasaki H, Kubo A, Amagai M, Matsui T, Kezic S. Filaggrin expression and processing deficiencies impair corneocyte surface texture and stiffness in mice. J Invest Dermatol. 2020;140 3:615–23.e5.
11. Jurakic TR, Kezic S, Jakasa I, Ljubojevic HS, Balic A, Petkovic M, Pavicic B, Zuzul K, Marinovic B. Filaggrin loss-of-function mutations and levels of filaggrin degradation products in adult patients with atopic dermatitis in Croatia. J Eur Acad Dermatol Venereol. 2020.

12. Catunda R, Rekhi U, Clark D, Levin L, Febbraio M. Loricrin downregulation and epithelial-related disorders: a systematic review. J Dtsch Dermatol Ges. 2019;17 12:1227–38.
13. Ilves M, Palomäki J, Vippola M, Lehto M, Savolainen K, Savinko T, Alenius H. Topically applied ZnO nanoparticles suppress allergen induced skin inflammation but induce vigorous IgE production in the atopic dermatitis mouse model. Part Fibre Toxicol. 2014;11 1:38–8.
14. Wang M, Lai X, Shao L, Li L. Evaluation of immunoresponses and cytotoxicity from skin exposure to metallic nanoparticles. Int J Nanomedicine. 2018;13:4445–59.
15. Jeong SH, Kim HJ, Ryu HJ, Ryu WI, Park Y, Bae HC, Jang YS, Son SW. ZnO nanoparticles induce TNF-α expression via ROS-ERK-Egr-1 pathway in human keratinocytes. J Dermatol Sci. 2013;72 3:263–73.
16. Gao F, Ma N, Zhou H, Wang Q, Zhang H, Wang P, Hou H, Wen H, Li L. Zinc oxide nanoparticles-induced epigenetic change and G2/M arrest are associated with apoptosis in human epidermal keratinocytes. Int J Nanomedicine. 2016;11:3859–74.
17. Kocbek P, Teskac K, Kreft ME, Kristl J. Toxicological aspects of long-term treatment of keratinocytes with ZnO and TiO_2 nanoparticles. Small. 2010;6 17:1908–17.
18. Boehncke WH, Schon MP. Psoriasis. Lancet. 2015;386:9997:983–94.
19. Perera GK, Di Meglio P, Nestle FO. Psoriasis. Annu Rev Pathol. 2012;7:385–422.
20. Swindell WR, Michaels KA, Sutter AJ, Diaconu D, Fritz Y, Xing X, Sarkar MK, Liang Y, Tsoi A, Gudjonsson JE, Ward NL. Imiquimod has strain-dependent effects in mice and does not uniquely model human psoriasis. Genome Med. 2017;9:1:24.
21. van der Fits L, Mourits S, Voerman JS, Kant M, Boon L, Laman JD, Cornelissen F, Mus AM, Florencia E, Prens EP, Lubberts E. Imiquimod-induced psoriasis-like skin inflammation in mice is mediated via the IL-23/IL-17 axis. J Immunol. 2009;182 9:5836–45.
22. Bimczok R, Gers-Barlag H, Mundt C, Klette E, Bielfeldt S, Rudolph T, Pflucker F, Heinrich U, Tronnier H, Johncock W, Klebon B, Westenfelder H, Flosser-Muller H, Jenni K, Kockott D, Lademann J, Herzog B, Rohr M. Influence of applied quantity of sunscreen products on the sun protection factor–a multicenter study organized by the DGK Task Force Sun Protection. Skin Pharmacol Physiol. 2007;20 1:57–64.
23. Wu JK, Siller G, Strutton G. Psoriasis induced by topical imiquimod. Australas J Dermatol. 2004;45 1:47–50.
24. Vinter H, Iversen L, Steiniche T, Kragballe K, Johansen C. Aldara®-induced skin inflammation: studies of patients with psoriasis. Br J Dermatol. 2015;172(2):345–53.
25. Cai Z, Liu X, Wang X, Chen Z, Song Z, Xu Y, Tao H, Li Y, Chen R, Guo L, Fu F. Fluorescence imaging of Cys in keratinocytes upon UVB exposure using phenyl doped graphitic carbon nitride nanosheets-Au nanoparticles nanocomposite. Anal Chim Acta. 2019;1091:127–34.
26. Wu Y, Liu L, Bian C, Diao Q, Nisar MF, Jiang X, Bartsch JW, Zhong M, Hu X, Zhong JL. MicroRNA let-7b inhibits keratinocyte differentiation by targeting IL-6 mediated ERK signaling in psoriasis. Cell Commun Signal. 2018;16:1:58.

27. Moos S, Mohebiany AN, Waisman A, Kurschus FC. Imiquimod-induced psoriasis in mice depends on the IL-17 signaling of keratinocytes. J Invest Dermatol. 2019;139 5:1110–7.
28. El MK, Karbach SH, Huppert J, Zayoud M, Reissig S, Schuler R, Nikolaev A, Karram K, Munzel T, Kuhlmann CR, Luhmann HJ, von Stebut E, Wortge S, Kurschus FC, Waisman A. An alternative pathway of imiquimod-induced psoriasis-like skin inflammation in the absence of interleukin-17 receptor a signaling. J Invest Dermatol. 2013;133 2:441–51.
29. Bai L, Fang H, Xia S, Zhang R, Li L, Ochando J, Xu J, Ding Y. STAT1 activation represses IL-22 gene expression and psoriasis pathogenesis. Biochem Biophys Res Commun. 2018;501 2:563–9.
30. Bakry OA, Samaka RM, Shoeib MAM, Abdel Aal SM. Nuclear factor kappa B and cyclo-oxygenase-2: two concordant players in psoriasis pathogenesis. Ultrastruct Pathol. 2013;39 1:49–61.
31. Tee JK, Ong CN, Bay BH, Ho HK, Leong DT. Oxidative stress by inorganic nanoparticles. Wiley Interdiscip Rev Nanomed Nanobiotechnol. 2016;8 3:414–38.
32. Lu SC. Regulation of glutathione synthesis. Mol Aspects Med. 2009;1–2 30:42–59.
33. Lowes MA, Suarez-Farinas M, Krueger JG. Immunology of psoriasis. Annu Rev Immunol. 2014;32:227–55.
34. Gaur U, Aggarwal BB. Regulation of proliferation, survival and apoptosis by members of the TNF superfamily. Biochem Pharmacol. 2003;66 8:1403–8.
35. Yan S, Xu Z, Lou F, Zhang L, Ke F, Bai J, Liu Z, Liu J, Wang H, Zhu H, Sun Y, Cai W, Gao Y, Su B, Li Q, Yang X, Yu J, Lai Y, Yu XZ, Zheng Y, Shen N, Chin YE, Wang H. NF-κB-induced microRNA-31 promotes epidermal hyperplasia by repressing protein phosphatase 6 in psoriasis. Nat Commun. 2015;6:7652.
36. Muller A, Hennig A, Lorscheid S, Grondona P, Schulze-Osthoff K, Hailfinger S, Kramer D. IκBζ is a key transcriptional regulator of IL-36-driven psoriasis-related gene expression in keratinocytes. Proc Natl Acad Sci U S A. 2018;115 40:10088–93.
37. Scheurer M, Brands RC, El-Mesery M, Hartmann S, Muller-Richter U, Kubler AC, Seher A. The selection of NFκB inhibitors to block inflammation and induce sensitisation to FasL-induced apoptosis in HNSCC cell lines is critical for their use as a prospective cancer therapy. Int J Mol Sci. 2019;20:6.
38. Shin HM, Kim MH, Kim BH, Jung SH, Kim YS, Park HJ, Hong JT, Min KR, Kim Y. Inhibitory action of novel aromatic diamine compound on lipopolysaccharide-induced nuclear translocation of NF-kappaB without affecting IkappaB degradation. FEBS Lett. 2004;571(1–3):50–4.
39. Kundu J, Kim DH, Chae IG, Lee JK, Lee S, Jeong CH, Chun KS. Silicon dioxide nanoparticles induce COX-2 expression through activation of STAT3 signaling pathway in HaCaT cells. Toxicol In Vitro. 2018;52:235–42.
40. Jaeger A, Weiss DG, Jonas L, Kriehuber R. Oxidative stress-induced cytotoxic and genotoxic effects of nano-sized titanium dioxide particles in human HaCaT keratinocytes. Toxicology. 2012;296(1–3):27–36.
41. Tucci P, Porta G, Agostini M, Dinsdale D, Iavicoli I, Cain K, Finazzi-Agro A, Melino G, Willis A. Metabolic effects of TiO_2 nanoparticles, a common component of sunscreens and cosmetics, on human

keratinocytes. Cell Death Dis. 2013;4:e549.

42. Sabnam S, Pal A. Relevance of Erk1/2-PI3K/Akt signaling pathway in CEES-induced oxidative stress regulates inflammation and apoptosis in keratinocytes. Cell Biol Toxicol. 2019;35 6:541–64.
43. Atkuri KR, Mantovani JJ, Herzenberg LA, Herzenberg LA. N-Acetylcysteine–a safe antidote for cysteine/glutathione deficiency. Curr Opin Pharmacol. 2007;7 4:355–9.
44. Arfsten DP, Johnson EW, Wilfong ER, Jung AE, Bobb AJ. Distribution of radio-labeled N-Acetyl-L-Cysteine in Sprague-Dawley rats and its effect on glutathione metabolism following single and repeat dosing by oral gavage. Cutan Ocul Toxicol. 2007;26:2:113–34.
45. Samuni Y, Goldstein S, Dean OM, Berk M. The chemistry and biological activities of N-acetylcysteine. Biochim Biophys Acta. 2013;1830 8:4117–29.
46. Sato H, Tamba M, Ishii T, Bannai S. Cloning and expression of a plasma membrane cystine/glutamate exchange transporter composed of two distinct proteins. J Biol Chem. 1999;274 17:11455–8.
47. McBean GJ, McBean GJ. The transsulfuration pathway: a source of cysteine for glutathione in astrocytes. Amino Acids. 2012;42 1:199–205.
48. Lee E, Kim H, Lee M, Jin SH, Hong SH, Ahn S, Kim SO, Shin DW, Lee S, Noh M. Cystathionine metabolic enzymes play a role in the inflammation resolution of human keratinocytes in response to sub-cytotoxic formaldehyde exposure. Toxicol Appl Pharmacol. 2016;310:185–94.
49. Belalcázar AD, Ball JG, Frost LM, Valentovic MA, Wilkinson JT. Transsulfuration is a significant source of sulfur for glutathione production in human mammary epithelial cells. ISRN Biochem. 2014;2013:637897.
50. Ferreira L, Dos RS, Do NDSE, Cadore S, Bernardes J, Durán N, de Jesus MB. Thiol-antioxidants interfere with assessing silver nanoparticle cytotoxicity. Nanomedicine. 2020;24:102130.
51. Karadottir H, Coorens M, Liu Z, Wang Y, Agerberth B, Giske CG, Bergman P. Klebsiella pneumoniae expressing VIM-1 metallo-β-lactamase is resensitized to cefotaxime via thiol mediated zinc chelation. Infect Immun. 2019;88:1.

Tables

Table 1. Primer sequences specific for mice used in the qRT-PCR analysis

Gene	Forward primer	Reverse primer
TNF-α	AGGCACTCCCCCAAAGATG	GCTCCTCCACTTGGTGGTTT
IL-1β	TGCCACCTTTTGACAGTGATG	ATGTGCTGCTGCGAGATTTG
IL-6	TTGCCTTCTTGGGACTGATG	CAGAATTGCCATTGCACAACTC
IL-17A	CAAAGCTCAGCGTGTCCAAAC	CTATCAGGGTCTTCATTGCGG
IL-22	GCGGTGACGACCAGAACATC	GGAAGGAGCAGTTCTTCGTTTTC
GAPDH	CTTCGGGCCACGCTAATCTC	ATGAAGGGGTCGTTGATGGC

Table 2. Primer sequences specific for human used in the qRT-PCR analysis

Gene	Forward primer	Reverse primer
TNF-α	CGAGTGACAAGCCTGTAGCC	CCTTGAAGAGGACCTGGGAGT
IL-1β	CACTACAGCAAGGGCTTCAGG	TGATCGTACAGGTGCATCGTG
IL-6	AATGAGGAGACTTGCCTGGTG	CTGGCATTTGTGGTTGGGTC
IL-17A	TCTGTGATCTGGGAGGCAAAG	CCCACGGACACCAGTATCTTC
IL-22	GGGAGAAACTGTTCCACGGAG	TGACATGTGCTTAGCCTGTTGC
GAPDH	AGGTCGGTGTGAACGGATTTG	TGTAGACCATGTAGTTGAGGTCA

Table 3. Physicochemical properties of ZnO NPs used in this study

Composition	Morphology	Primary size (nm)	Hydrodynamic size (nm)	Zeta potential (mV)	Surface area (m^2/g)
ZnO NPs	Hexagonal	41.34 ± 9.41 [a]	810.3 ± 116.5 [b]	13.1 ± 0.5 [b]	27.3
			189.0 ± 63.3 [c]	11.9 ± 0.9 [c]	
			266.7 ± 69.2 [d]	10.9 ± 0.2 [d]	

[a] The primary nanoparticle size was measured by Image J software.

[bcd] The NPs were respectively dispersed in the suspensions used for animal experiments, complete medium or DW.

Figures

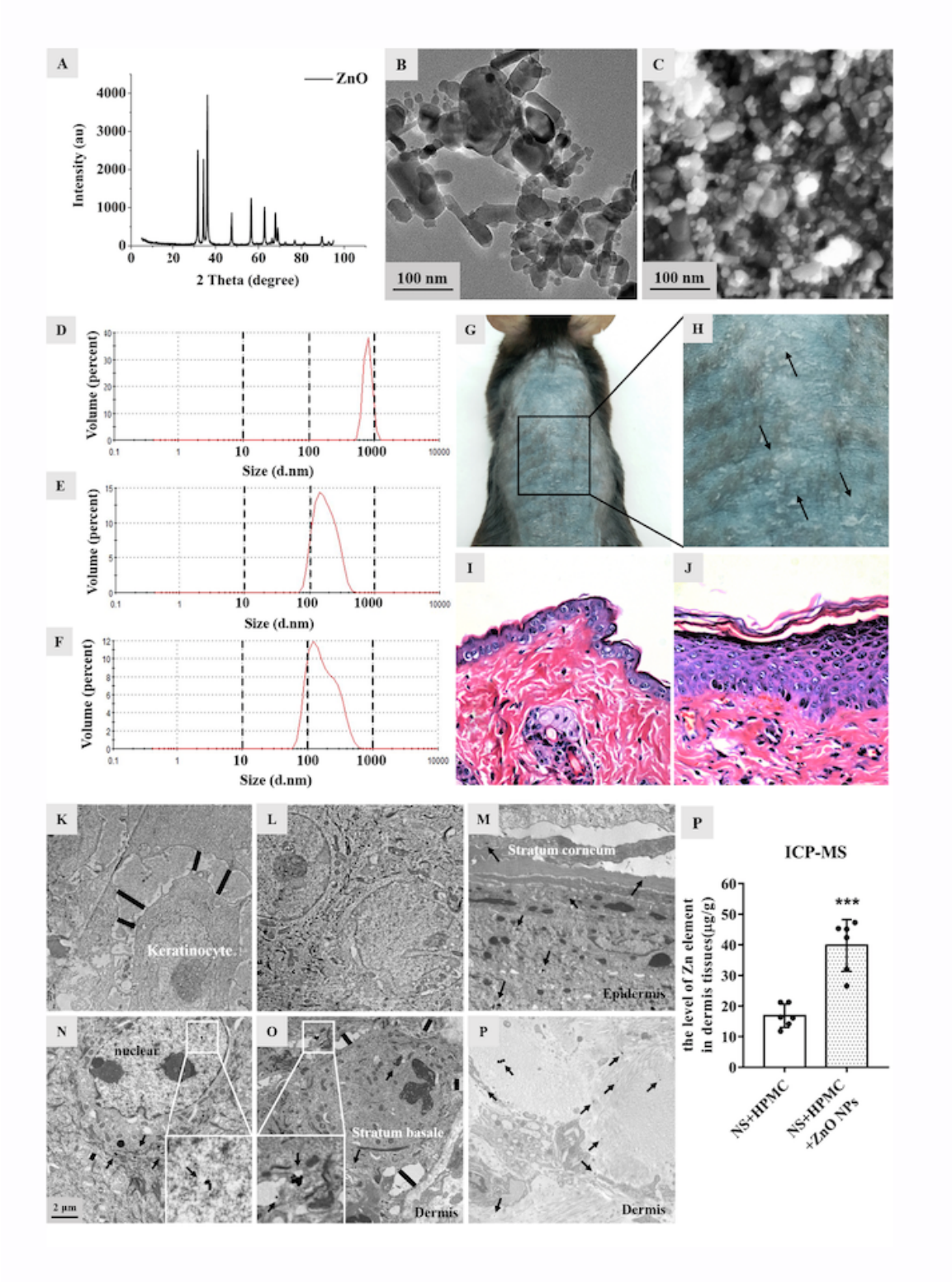

Figure 1

Characterization of ZnO NPs and penetration of ZnO NPs into skin. (A) XPS data identified the composition of ZnO NPs. (B~C) TEM image and SEM image of ZnO NPs. DLS datum showed the hydrodynamic sizes of ZnO NPs in the suspensions used for the animal experiments (D), complete medium (E) and DW (F). (G~H) Appearance of the dorsal skin treated with IMQ for 6 consecutive days (black arrows show scales). (I~J) H&E images (40×) of normal epidermis and the hyperplastic epidermis

induced by IMQ. (K) TEM image (12000×) of epidermal cells in psoriasis-like skin (black lines show intercellular gaps about 2000 nm). (L) After treatment with suspension without ZnO NPs for 3 consecutive days, the morphology of keratinocytes returned to normal and those wide intercellular gaps disappeared. (M~O) After treatment with suspension containing ZnO NPs for 3 consecutive days, ZnO NPs (as black arrows showed) entered epidermis through stratum corneum and were discovered in the nuclear of keratinocytes, stratum basale of epidermis and dermis, and the wide intercellular gaps remained. (P) ICP-MS analysis showed that elemental Zn content in the dermis of the ZnO NP-treated group was higher than in the negative control group (***P□0.001, n=6). Abbreviations: ZnO NPs: zinc oxide nanoparticles; XPS: X-ray photoelectron spectra; TEM: transmission electron microscopy; SEM: scanning electron microscopy; DLS: dynamic laser light scattering; DW: diluted water; IMQ: imiquimod; H&E: hematoxylin & eosin; ICP MS: inductively coupled plasma mass spectra.

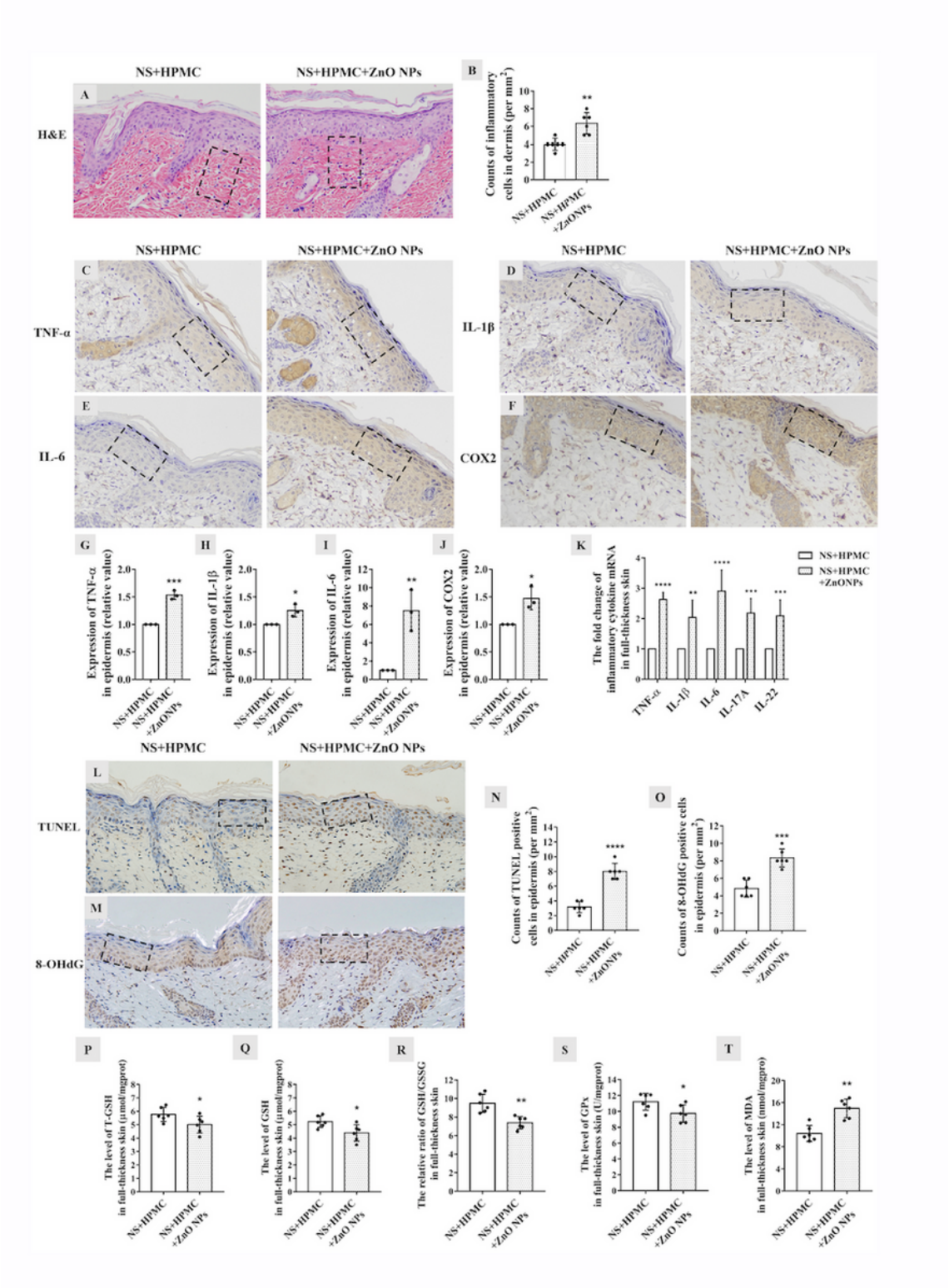

Figure 2

Histopathological examinations of inflammation response and measurements of oxidative stress in mice. (A~B) H&E staining showed that the number of inflammatory cells in the dermis was increased in the ZnO NP-treated group (n=6). (D~J) IHC evaluations showed that the expression levels of TNF-α, IL-1β, IL-6 and COX2 in epidermis were increased in the ZnO NP-treated group (n=3). (K) The mRNA levels of TNF-α, IL-1β, IL-6, IL-17A and IL-22 in the full-thickness skin were increased in the ZnO NP-treated group

(n=6). (L&N) The rate of positive TUNEL stanning was increased in the ZnO NP-treated group (n=6). (M&O) The rate of positive 8-OHdG stanning was increased in the ZnO NP-treated group, and in the negative control group, the positive cells were distributed mainly in the basal layer of epidermis, but in the ZnO NP-treated group, the positive cells were distributed in all layer of epidermis (n=6). (P~S) The levels of T-GSH, GSH and GPx as well as the ratio of GSH/GSSG in the full-thickness skin were decreased in the ZnO NP-treated group. (T) The MDA content in the full-thickness skin was decreased in the ZnO NP-treated group. (The area of each dotted rectangle is 2 mm2. *P<0.05, ** P<0.01, ***P<0.001, ****P<0.0001, n=6) Abbreviations: IHC: immunohistochemistry; TUNEL: TdT-mediated dUTP nick-end labelling; 8-OHdG: 8-hydroxy-2 deoxyguanosine; T-GSH: total glutathione; GSH: reduced glutathione; GSSG: oxidative glutathione; GPx: glutathione peroxidase; MDA: malondialdehyde.

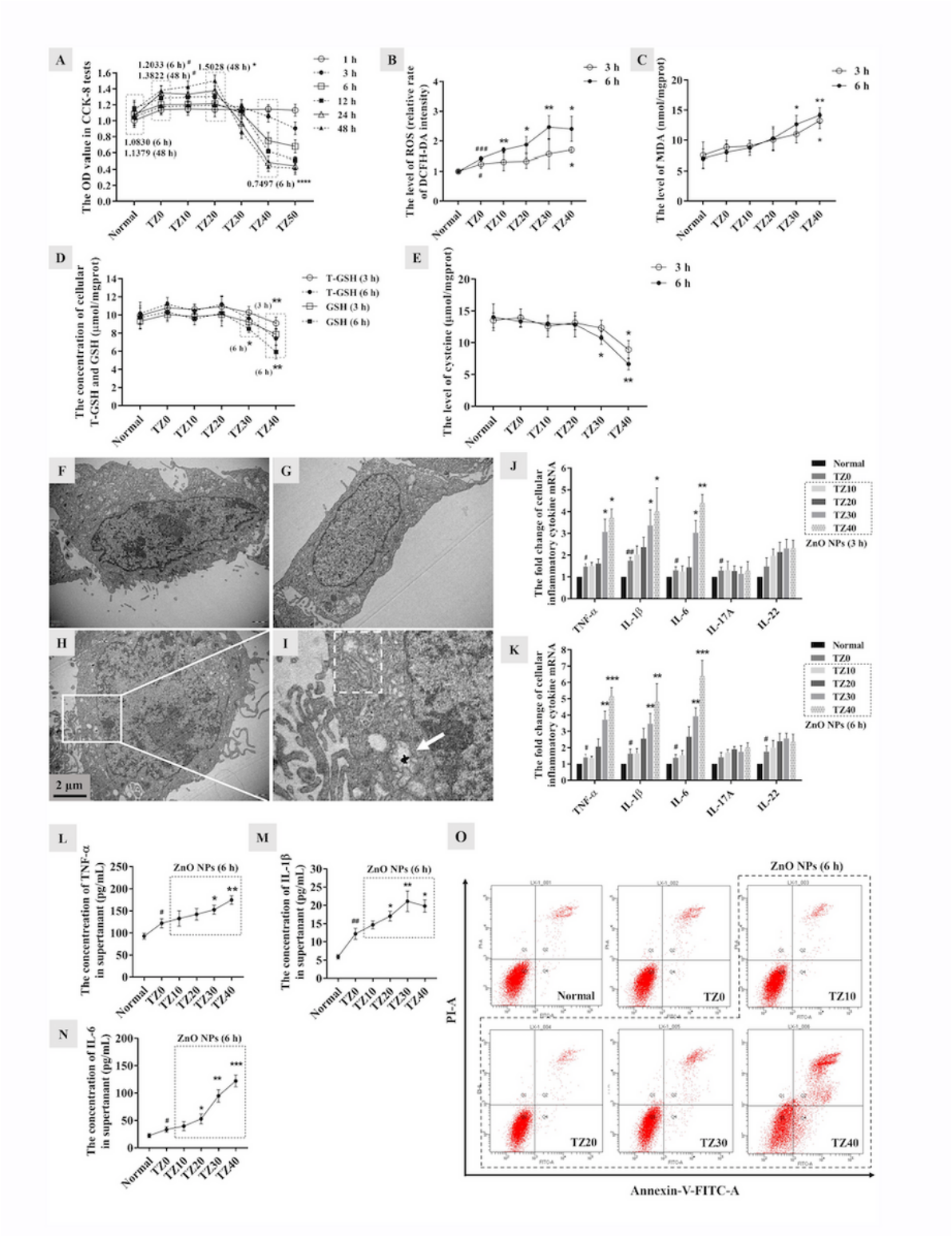

Figure 3

ZnO NP-induced alterations in redox homeostasis, inflammation and apoptosis in rh-TNF-α-stimulated HaCaT cells. (A) The rh-TNF-α-stimulated HaCaT cells were treated with ZnO NPs at dose of 0, 10, 20, 30 or 40 μg/mL for 1, 3, 6, 12, 24 or 48h, and CCK-8 tests showed that ZnO NPs decreased cell viability in a predominantly dose-dependent manner (n=6). (B) ZnO NPs increased the level of cellular ROS, detected by FCM. (C~E) ZnO NPs increased the level of MDA and decreased the levels of T-GSH, GSH and cysteine

at the dose of 30 or 40 μg/mL for 3 or 6 h. (F) TEM image of a normal HaCaT cell. (G) TEM image of a HaCaT cell stimulated by rh-TNF-α (10 ng/mL for 48 h). (H) TEM image of a rh-TNF-α-stimulated HaCaT cell exposed to ZnO NPs (40 μg/mL for 6 h). (I) ZnO NPs were engulfed by a rh-TNF-α-stimulated HaCaT cell (as shown by the white arrow) and caused changes in mitochondrial morphology (as the dotted rectangle showed). (J~K) ZnO NPs increased the mRNA levels of TNF-α, IL-1β and IL-6 at the dose of 30~40 μg/mL; (L~N) ZnO NPs promoted the secretion of TNF-α, IL-1β and IL-6 at the dose of 20~40 μg/mL; (O) ZnO NPs increased the number of apoptotic cells in Annexin-V/PI staining (Q3 represents normal cells; Q4 represents early apoptotic cells; and Q2 represents late apoptotic or necrotic cells). (# compared to normal HaCaT cells, * compared to the rh-TNF-α-stimulated HaCaT cells (TZ0). (# compared to normal HaCaT cells, * compared to the rh-TNF-α-stimulated HaCaT cells (TZ0). TZ10, TZ20, TZ30 or TZ40 means the treatment with ZnO NPs at the dose of 10, 20, 30 or 40 μg/mL. # or *P<0.05, ## or **P<0.01, ***P<0.001, ****P<0.0001, n=3) Abbreviations: rh-TNF-α: recombinant human TNF-α; FCM: flow cytometry.

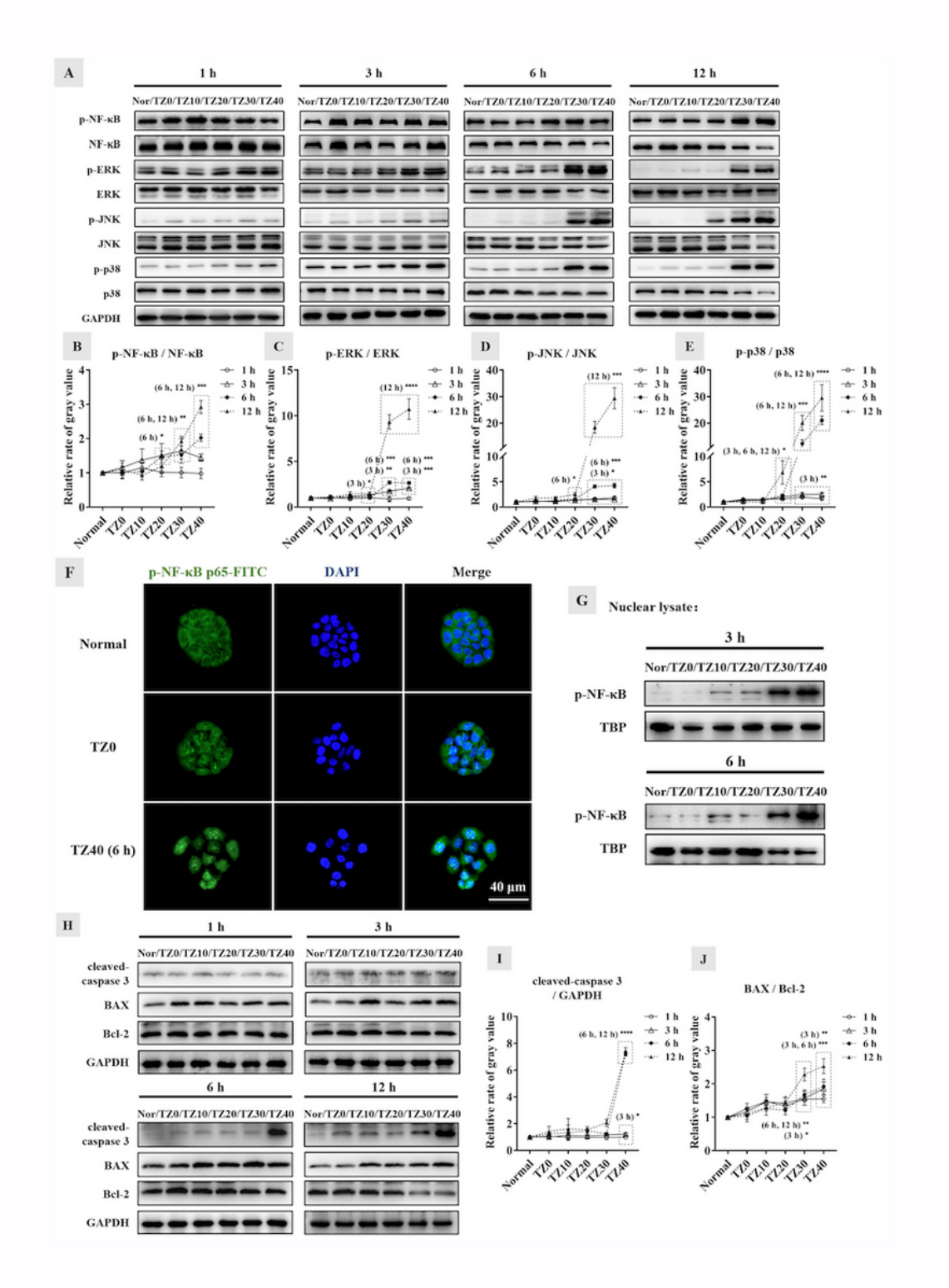

Figure 4

ZnO NP-induced alterations in signal pathways related to inflammation and apoptosis. (A) Western blotting in the total protein showed that ZnO NPs (0~40 μg/mL for 1~12 h) altered phosphorylation of NF-κB, ERK, p38 and JNK in a dose-and-time-dependent manner. (B~E) The gray value analysis showed that ZnO NPs (20~40 μg/mL for 3~12 h) promoted the phosphorylation of NF-κB, ERK, JNK and p38 in total protein. (F) Fluorescent images showed that rh-TNF-α stimulation promoted the nuclear

translocation of p-NF-κB p65, and ZnO NPs (40 μg/mL for 6 h) induced a strong nuclear translocation of p-NF-κB p65. (G) ZnO NPs (30 or 40 μg/mL for 3 or 6 h) significantly increased the level of p-NF-κB p65 in nuclear protein (compared to the TBP, a nuclear reference protein). (H~J) ZnO NPs (40 μg/mL for 3~12 h) significantly increased the level of cleaved-caspase 3 and the ratio of BAX/Bcl-2 in total protein. (* compared to the rh-TNF-α stimulated HaCaT cells (TZ0). *P<0.05, **P<0.01, ***P<0.001, ****P<0.0001, n=3) Abbreviations: NF-κB: nuclear factor-κB; p-NF-κB: phosphorylated NF-κB; ERK: extracellular regulated protein kinases; JNK: c-Jun N-terminal kinase; TBP, TATA-binding protein.

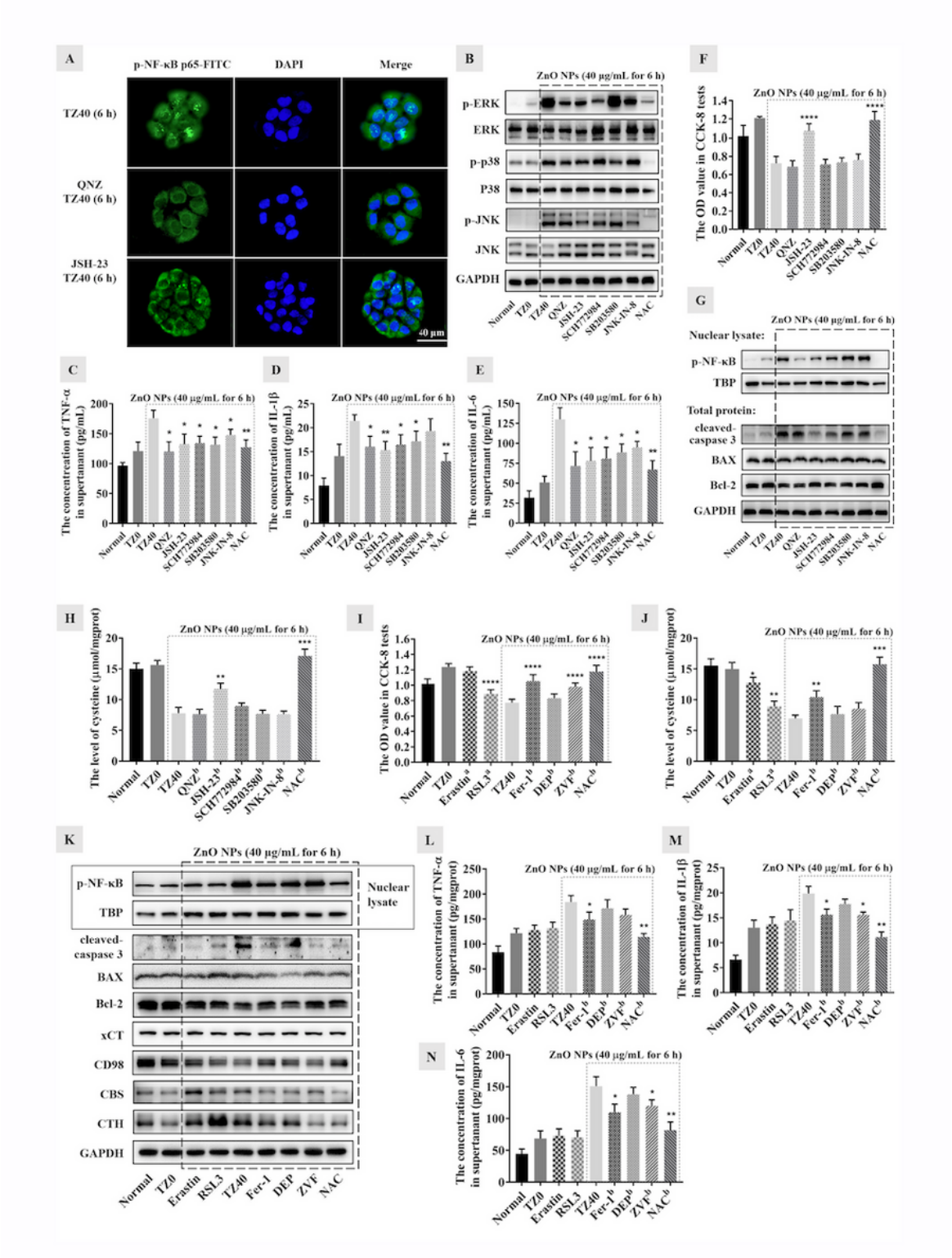

Figure 5

Effects of inhibitors of signalling pathways and antioxidants on ZnO NP-induced inflammation and apoptosis. (A) Fluorescent images showed that QNZ (0.1 μM) and JSH-23 (10 μM) inhibited ZnO NP-induced nuclear translocation of p-NF-κB p65. (B) SCH772984 (10 μM), SB203580 (2 μM) and JNK-IN-8 (1 μM) inhibited ZnO NP-induced phosphorylation of ERK, p38 and JNK, respectively. (C~E) Inhibitors of NF-κB and MAPK pathways and NAC inhibited ZnO NP-induced secretion of TNF-α, IL-1β and IL-6, but JNK-IN-8 did not inhibit ZnO NP-induced secretion of IL-1β. (F) JSH-23 and NAC inhibited ZnO NPs-induced decline in cell viability. (G) QNZ, JSH-23 and NAC (1 mM) inhibited ZnO NP-induced increase of nuclear p-NF-κB p65; JSH-23 and NAC inhibited the activation of caspase-3 and the increased ratio of BAX/Bcl-2 induced by ZnO NP. (H) JSH-23 and NAC inhibited ZnO NPs-induced decline in cysteine content. (I) RSL3 (10 μM) decreased cell viability in rh-TNF-α stimulated HaCaT cells but Erastin (200 μM) did not; Fer-1 (20 μM), ZVF (30 μM) and NAC inhibited ZnO NPs-induced decline in cell viability (n=6). (J) Erastin and RSL3 decreased cysteine content; Fer-1 and NAC inhibited ZnO NPs-induced decline in cysteine content. (K) Effects of Erastin and RSL3 on nuclear translocation of p-NF-κB p65 and the pathways related to apoptosis (the level of cleaved-caspase 3 and the ratio of BAX/Bcl-2) and cysteine synthesis (main pathway: xCT and CD98, transsulfuration pathway: CBS and CTH); and the effects of antioxidants and VZF on ZnO NP-induced alterations in those pathways. (L~N) Fer-1 and NAC inhibited ZnO NP-induced secretion of TNF-α, IL-1β and IL-6; ZVF inhibited ZnO NP-induced secretion of IL-1β and IL-6. (a compared to TZ0, b compared to TZ40. *P<0.05, ** P<0.01, ***P<0.001, ****P<0.0001, n=3) Abbreviations: MAPK: mitogen-activated protein kinase (including p-44/42 MAPK (ERK), p38 MAPK and JNK), NAC: N-acetylcysteine; Fer-1: ferrostatin-1, DEP: deferiprone, ZVF: Z-VAD-FMK, CBS: cystathionine β-synthase, CTH: γ-cystathionase.